Supplementary Information

Fine-tuned ultramicroporous carbon materials via CO_2 activation for molecular sieving of fluorinated propylene and propane

Yiwen Fu,[†ab] Liangzheng Sheng,[†a] Wei Xia,[a] Guangtong Hai,[*ab] Jialei Yan,[a] Lihang Chen,[*ab] Qiwei Yang,[ab] Zhiguo Zhang,[ab] Qilong Ren,[ab] and Zongbi Bao,[*ab]

[a] *Key Laboratory of Biomass Chemical Engineering of ministry of Education, College of Chemical and Biological Engineering, Zhejiang University, 38 Zheda Road, Hangzhou 310027, P. R. China.*

[b] *Zhejiang Key Laboratory of F-contained Functional Materials, Institute of Zhejiang University-Quzhou, 99 Zheda Road, Quzhou 324000, PR China.*

[†] These authors contributed equally to this work.

* Corresponding authors.

E-mail address: baozb@zju.edu.cn; chenlihang@zju.edu.cn; haigt@zju.edu.cn.

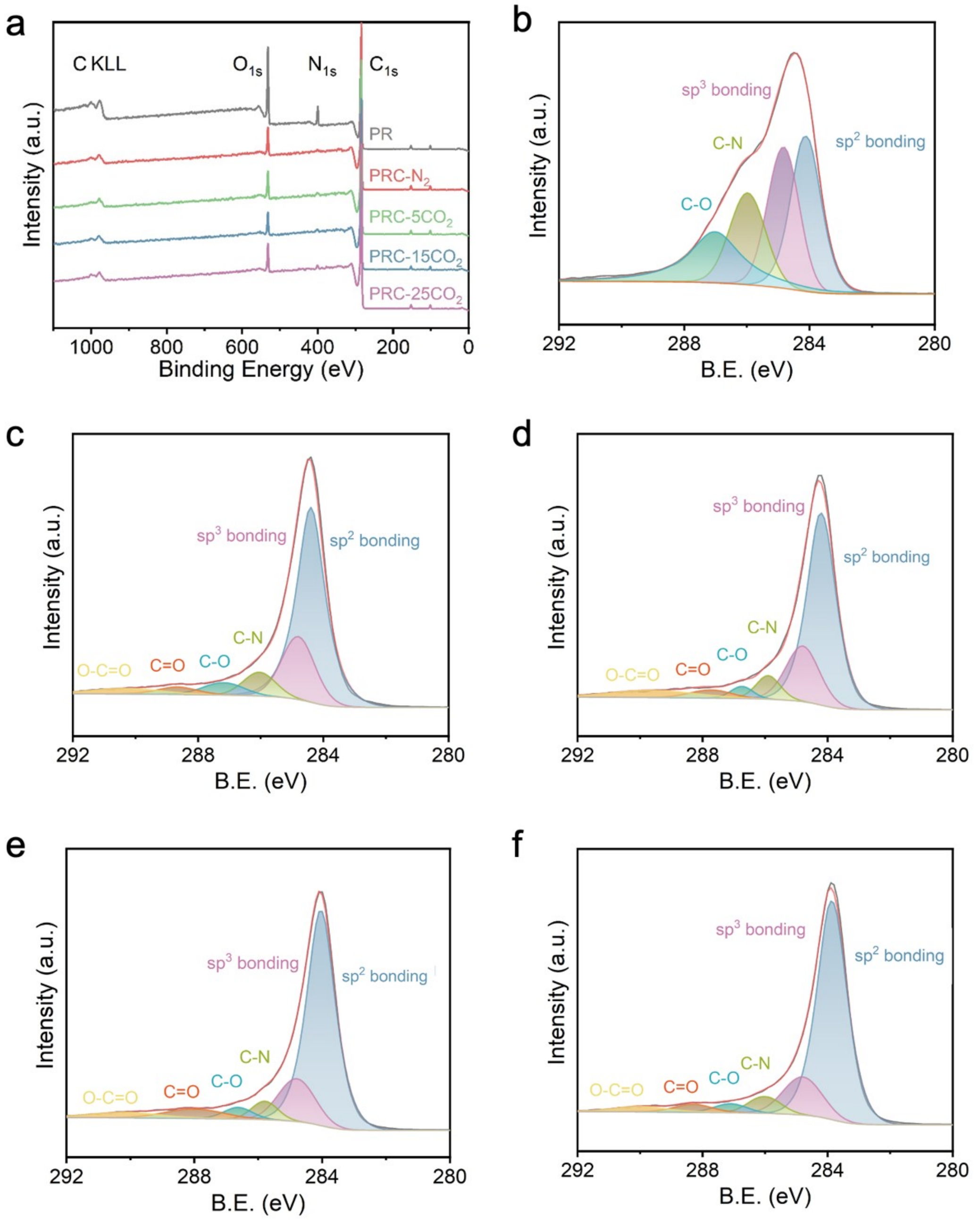

Fig. S1 XPS spectra of precursor PR and its derived carbon molecular sieve materials: (a) XPS spectra; High-resolution spectra of C_{1s} for (b) PR; (c) PRC-N_2; (d) PRC-5CO_2; (e) PRC-15CO_2; (f) PRC-25CO_2.

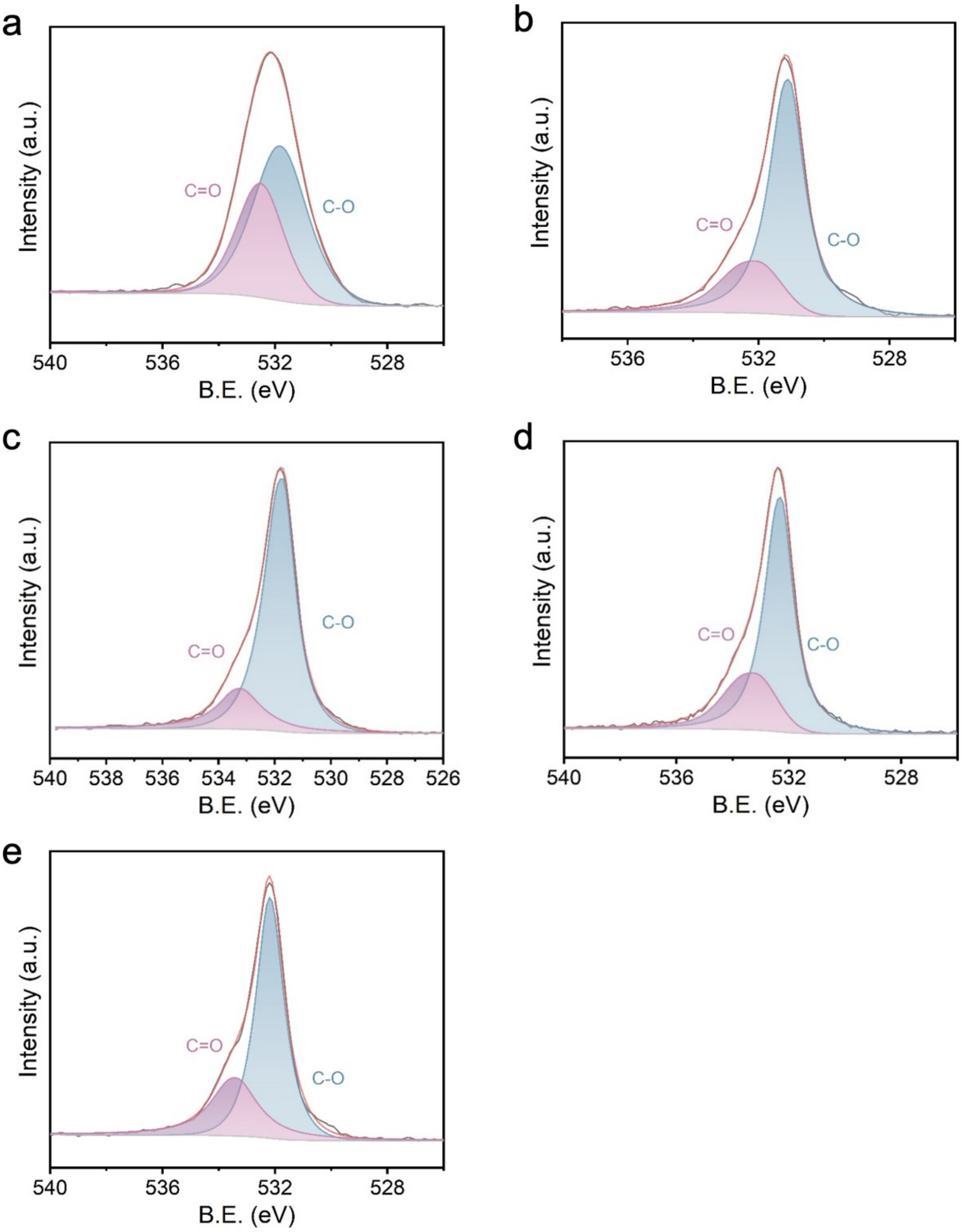

Fig. S2 High-resolution spectra of O_{1s} for (a) PR; (b) PRC-N_2; (c) PRC-5CO_2; (d) PRC-15CO_2; (e) PRC-25CO_2.

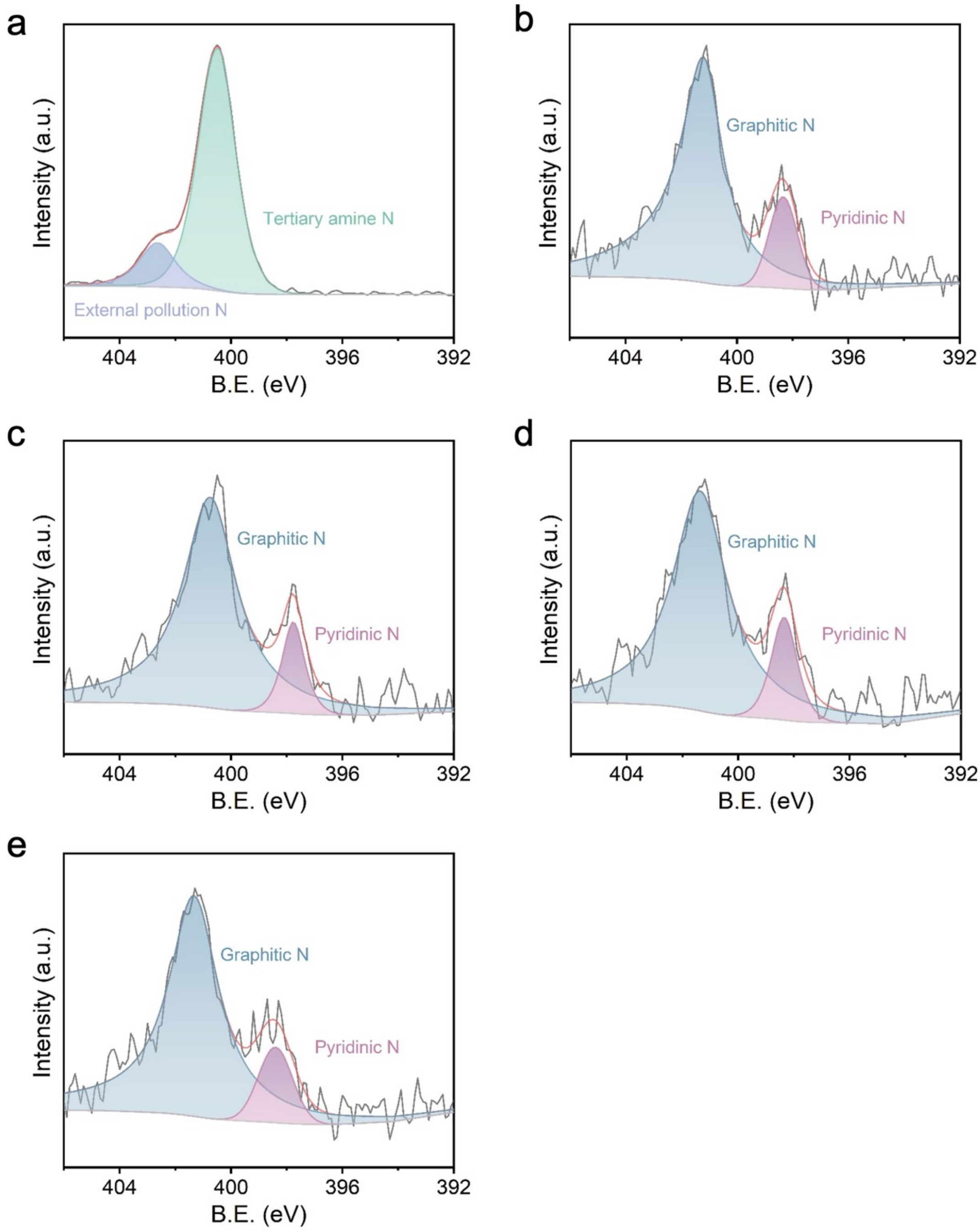

Fig. S3 High-resolution spectra of N_{1s} for (a) PR; (b) PRC-N_2; (c) PRC-5CO_2; (d) PRC-15CO_2; (e) PRC-25CO_2.

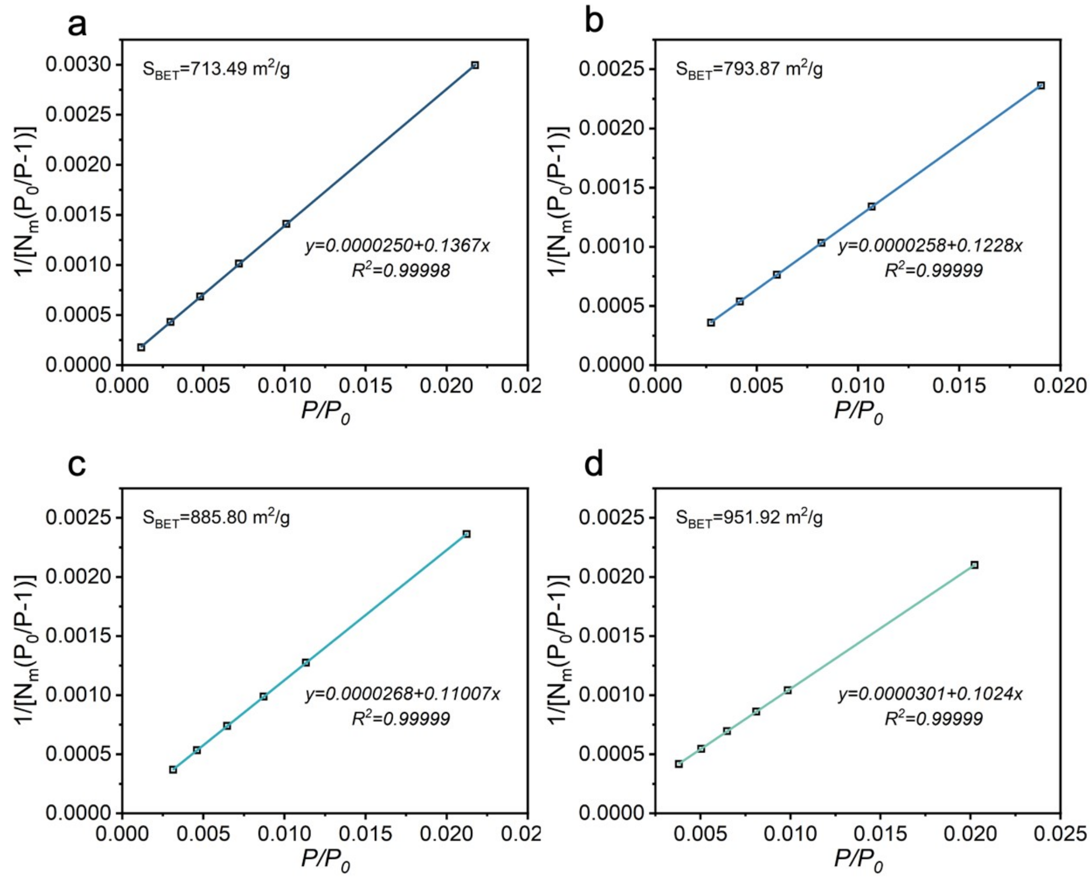

Fig. S4 Linear fitting of BET specific surface area of PR-derived carbon molecular sieve materials for (a) PRC-N_2; (b) PRC-5CO_2; (c) PRC-15CO_2; (d) PRC-25CO_2.

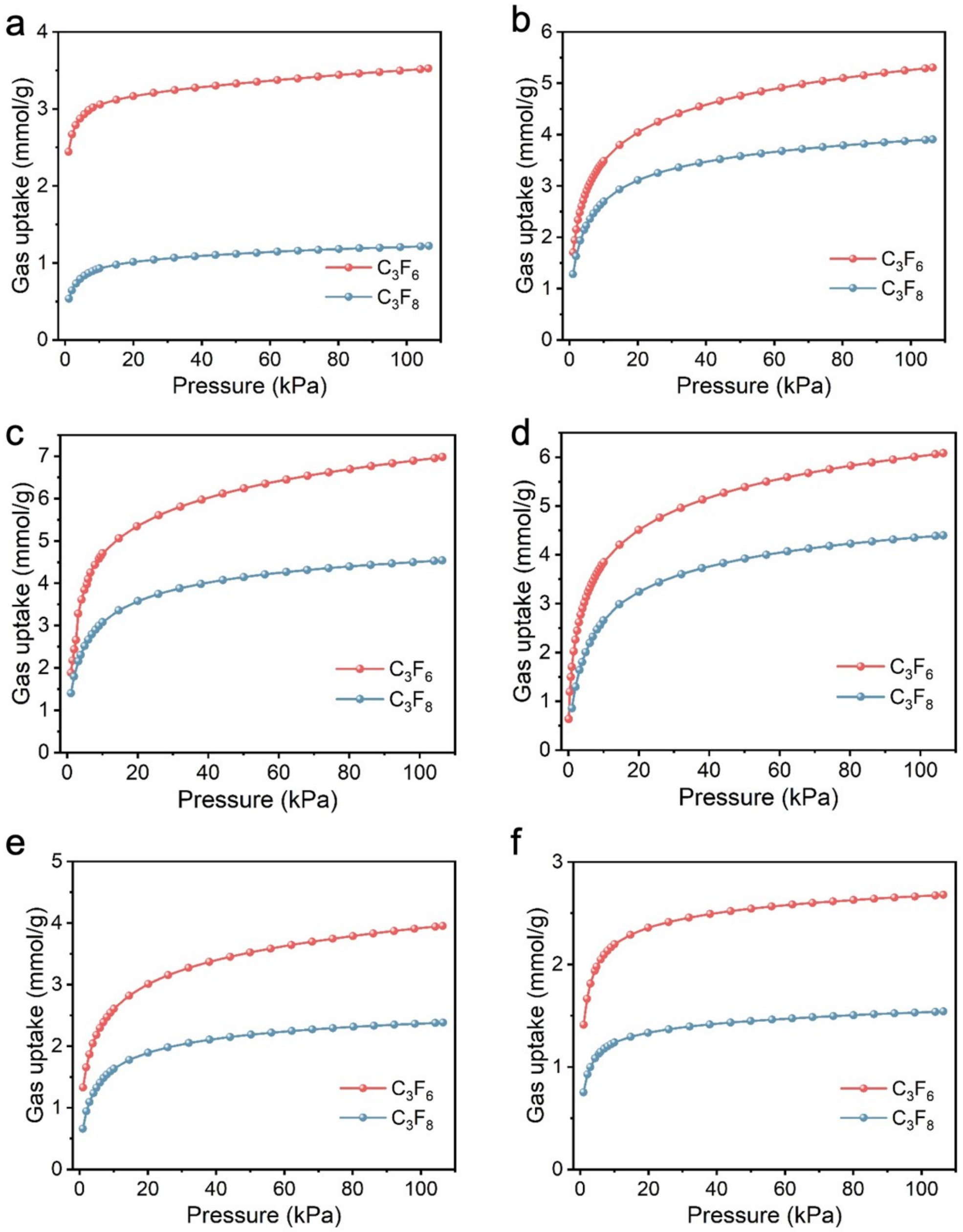

Fig. S5 Adsorption isotherms of C_3F_6 and C_3F_8 on commercial carbon material adsorbents at 298 K and 100 kPa: (a) AC1; (b) AC2; (c) AC3; (d) AC4; (e) AC5; (f) AC6.

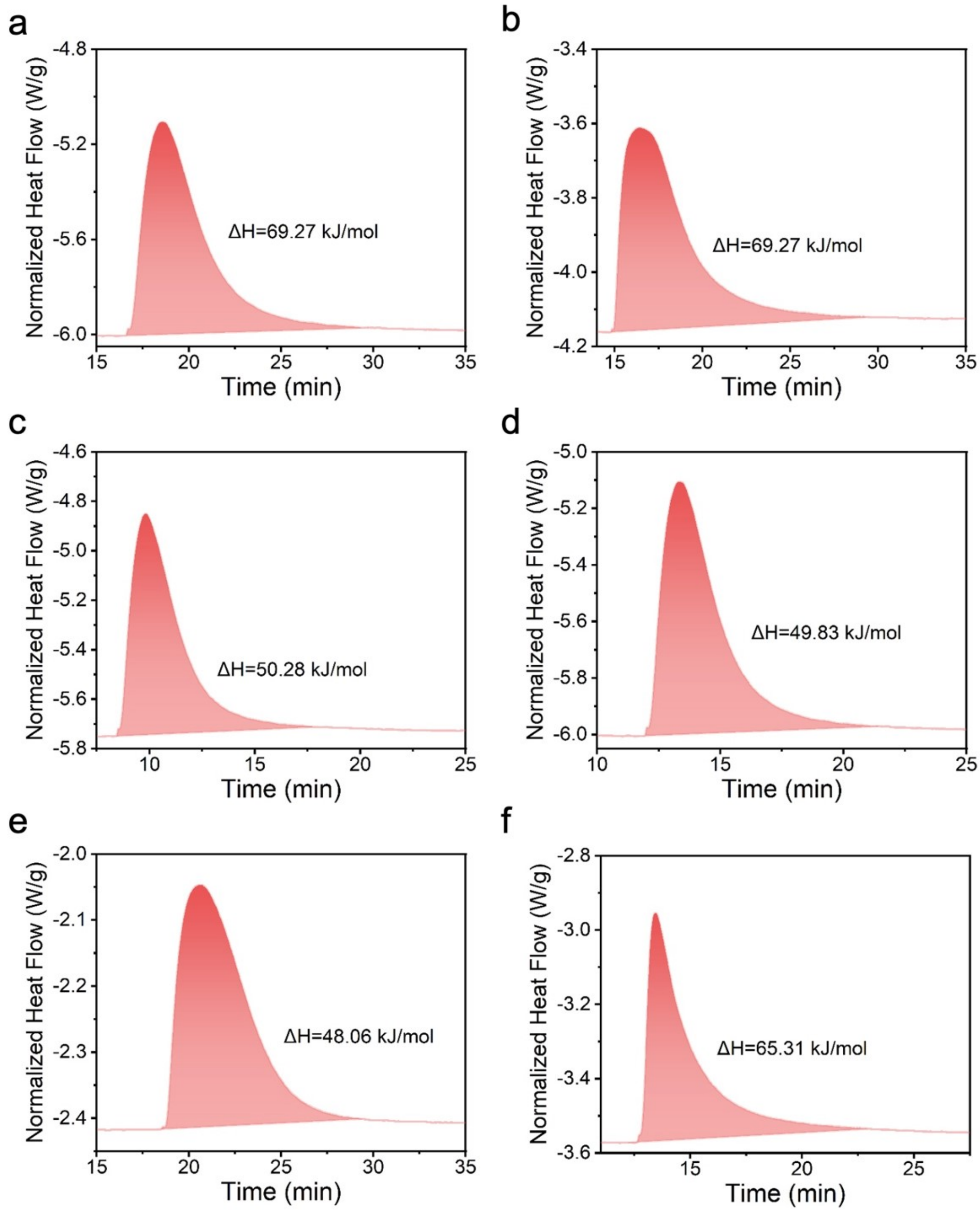

Fig. S6 Heats of adsorption by TG-DSC analysis of (a) AC1; (b) AC2; (c) AC3; (d) AC4; (e) AC5; (f) AC6.

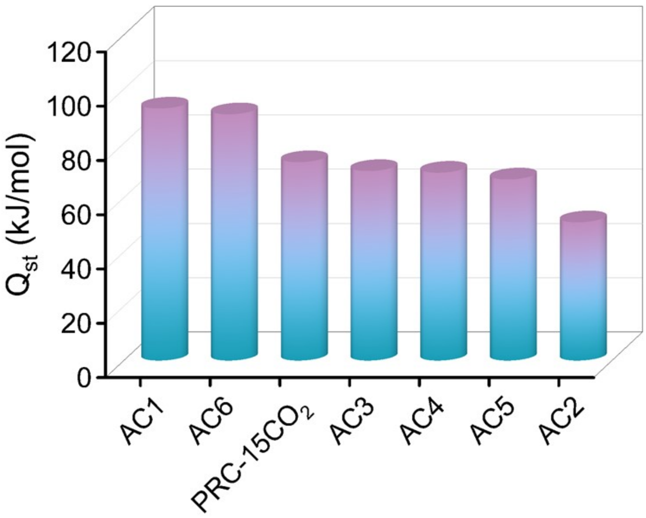

Fig. S7 Heats of adsorption by TG-DSC analysis of C_3F_6 on various carbon-based adsorbents.

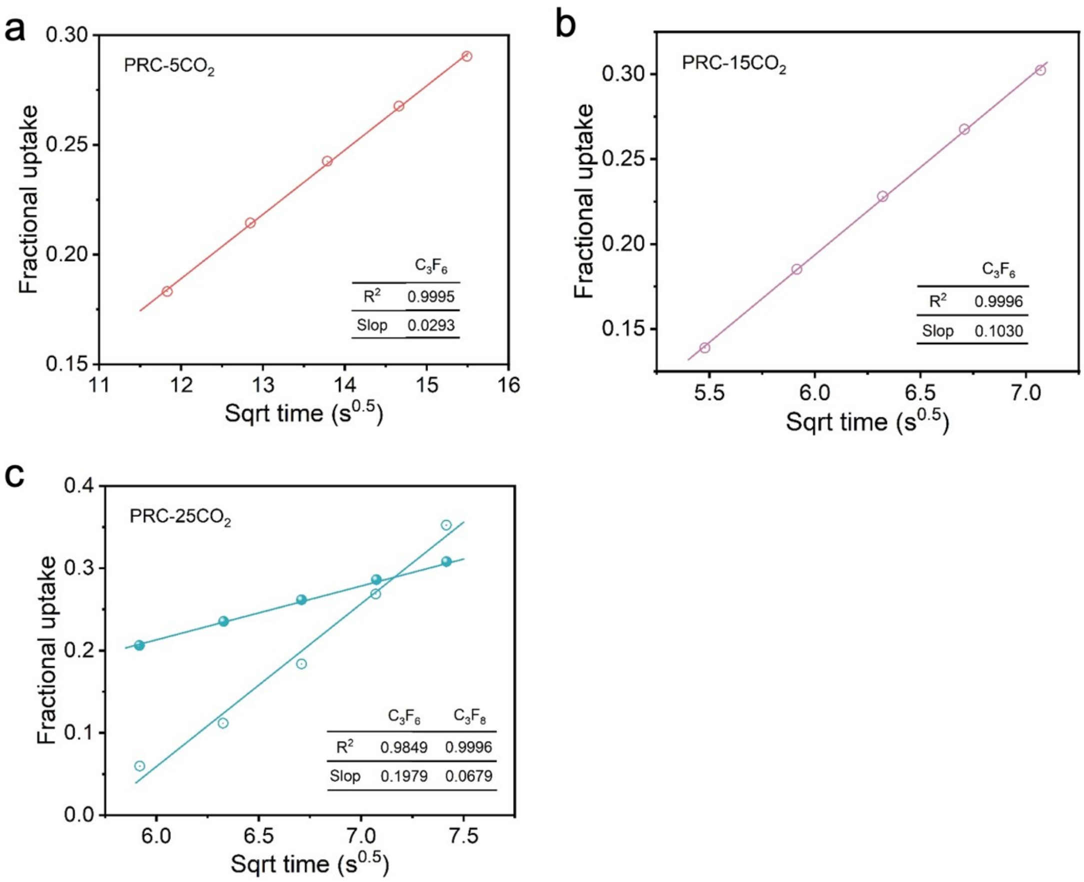

Fig. S8 Fitting of diffusion time constants of C_3F_6 and C_3F_8 on PR-derived carbon molecular sieve materials at 298 K and 100 kPa: (a) PRC-5CO_2, (b) PRC-15CO_2, (c) PRC-25CO_2.

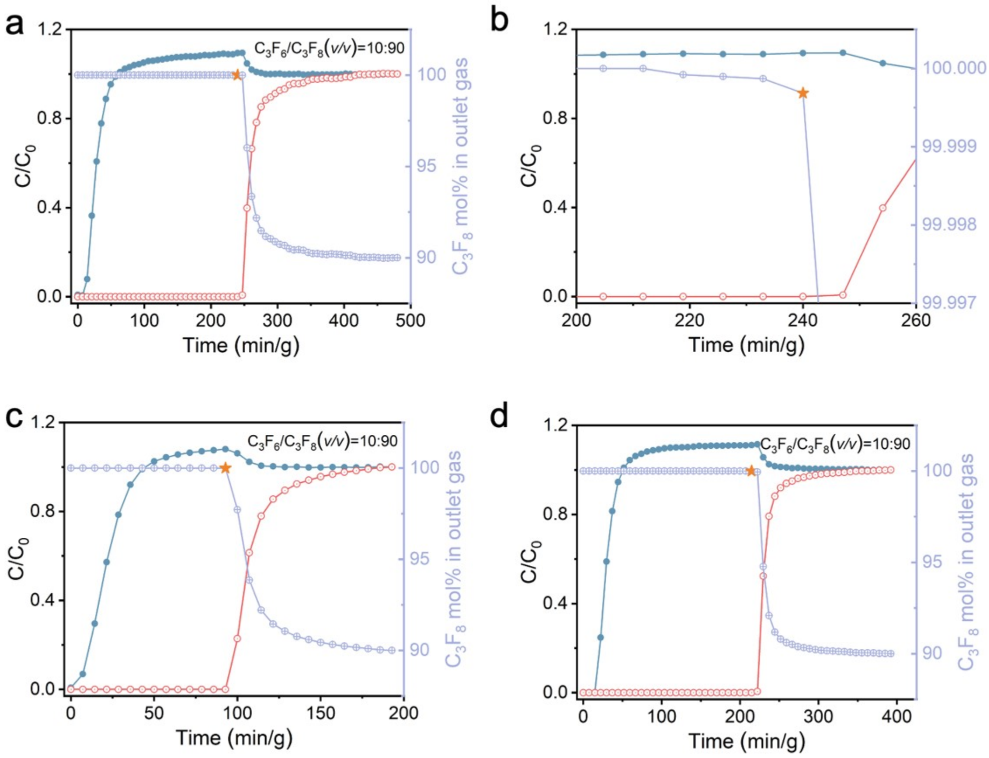

Fig. S9 Experimental breakthrough curves of C_3F_6/C_3F_8 (10/90, *v*/*v*) on PR-derived carbon molecular sieve materials at 298 K and 100 kPa: (a) PRC-15CO_2; (b) Partially enlarged contour plot of Fig S9a; (c) PRC-5CO_2; (d) PRC-25CO_2. The feed gas flow rate was 2.0 mL/min, The bright yellow pentagram indicates that the outlet purity of C_3F_8 is over 99.999% at this point.

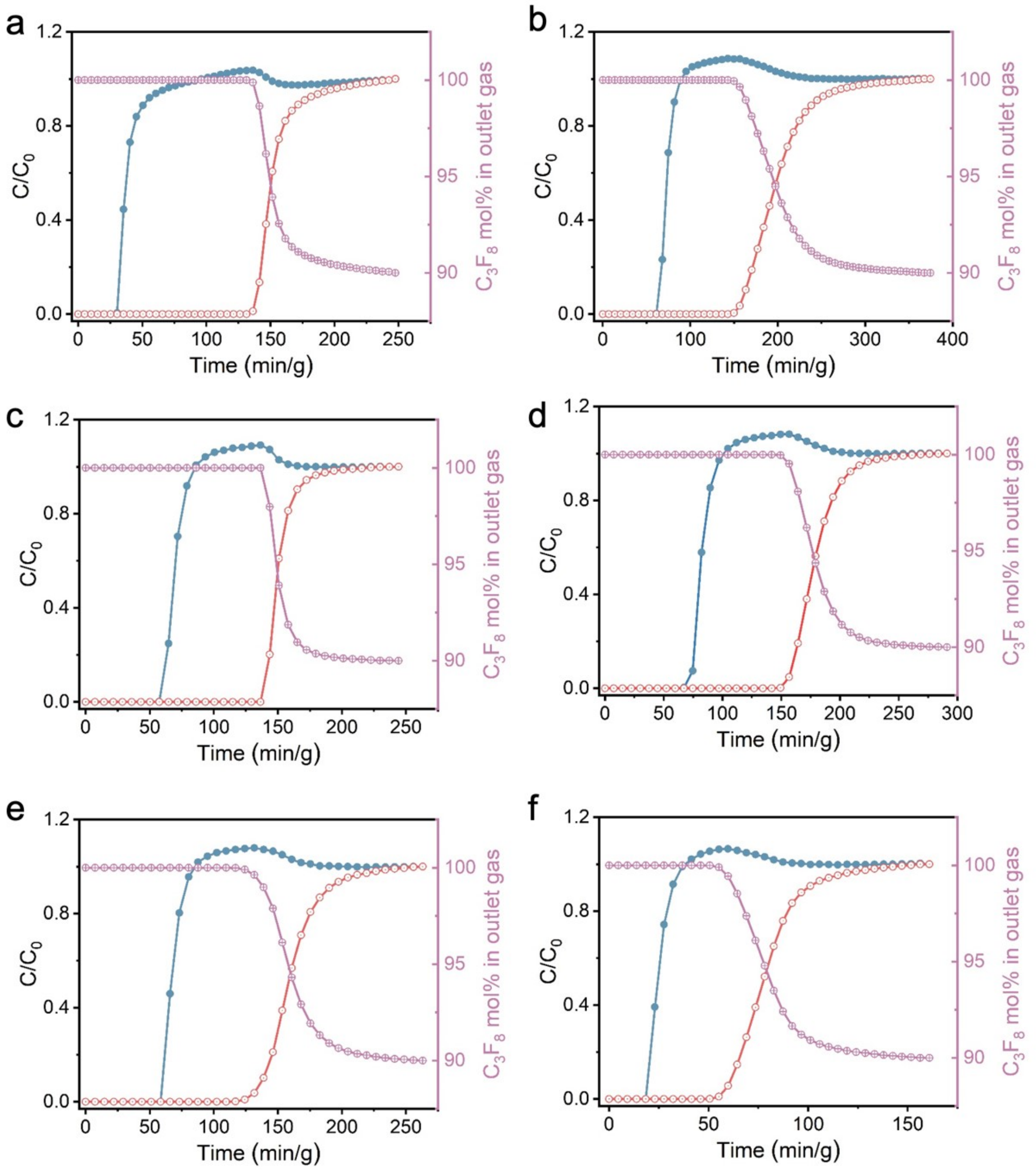

Fig. S10 Experimental curves of fixed-bed breakthrough of C_3F_6/C_3F_8 (10/90, *v/v*) gas mixtures on commercial carbon material adsorbents at 298 K and 100 kPa: (a) AC1; (b) AC2; (c) AC3; (d) AC4; (e) AC5; and (f) AC6. The flow rate of raw gas was 2.0 mL/min.

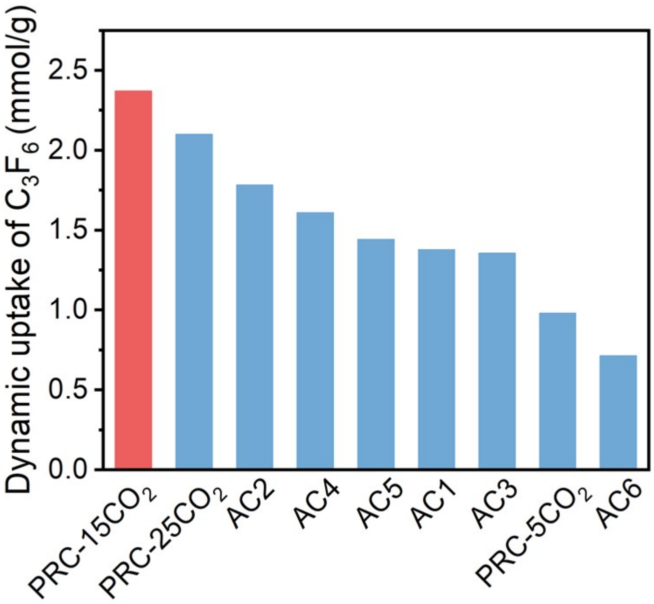

Fig. S11 Comparison of the separation performance of the above carbon-based adsorbents for C_3F_6/C_3F_8 (10/90, *v/v*) mixtures at 298 K and 100 kPa on the dynamic adsorption capacity of C_3F_6.

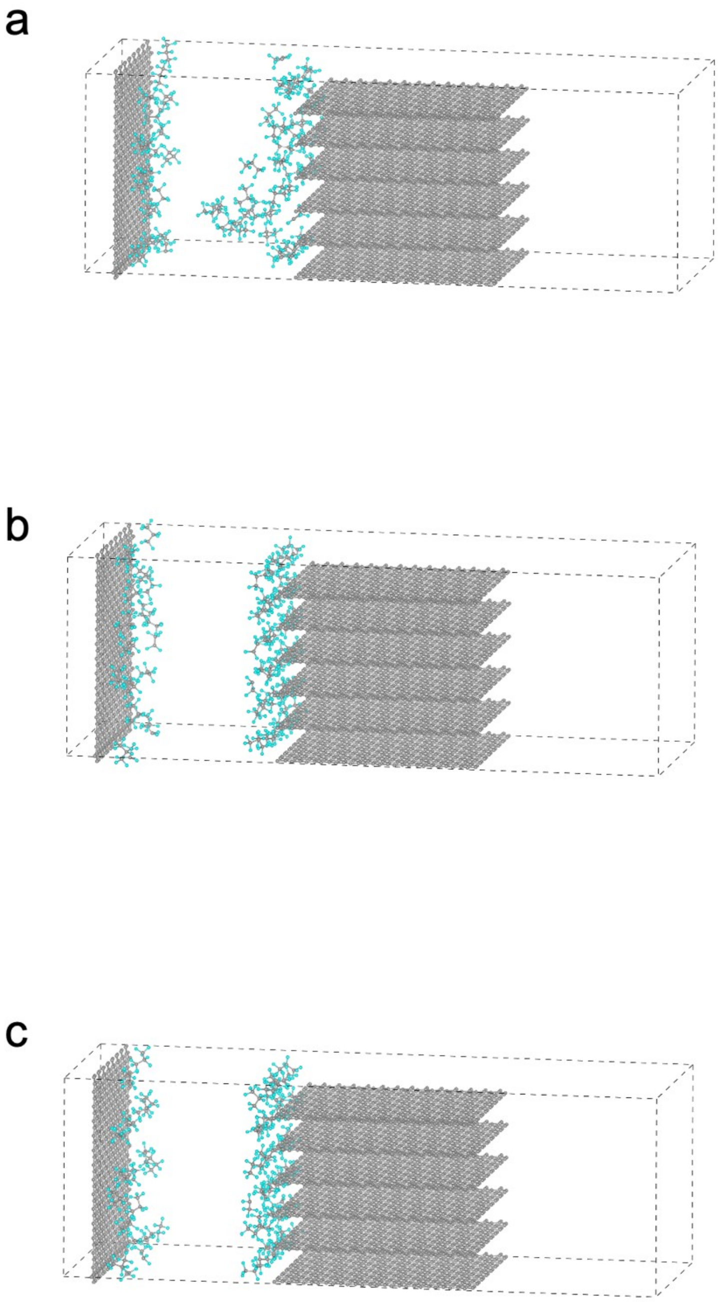

Fig. S12 The number of gas molecules that passed through the PRC-5CO_2 channels in the MD simulation as a function of simulation time: (a) 0 ps; (b) 50 000 ps and (c) 100000 ps.

a

b

c

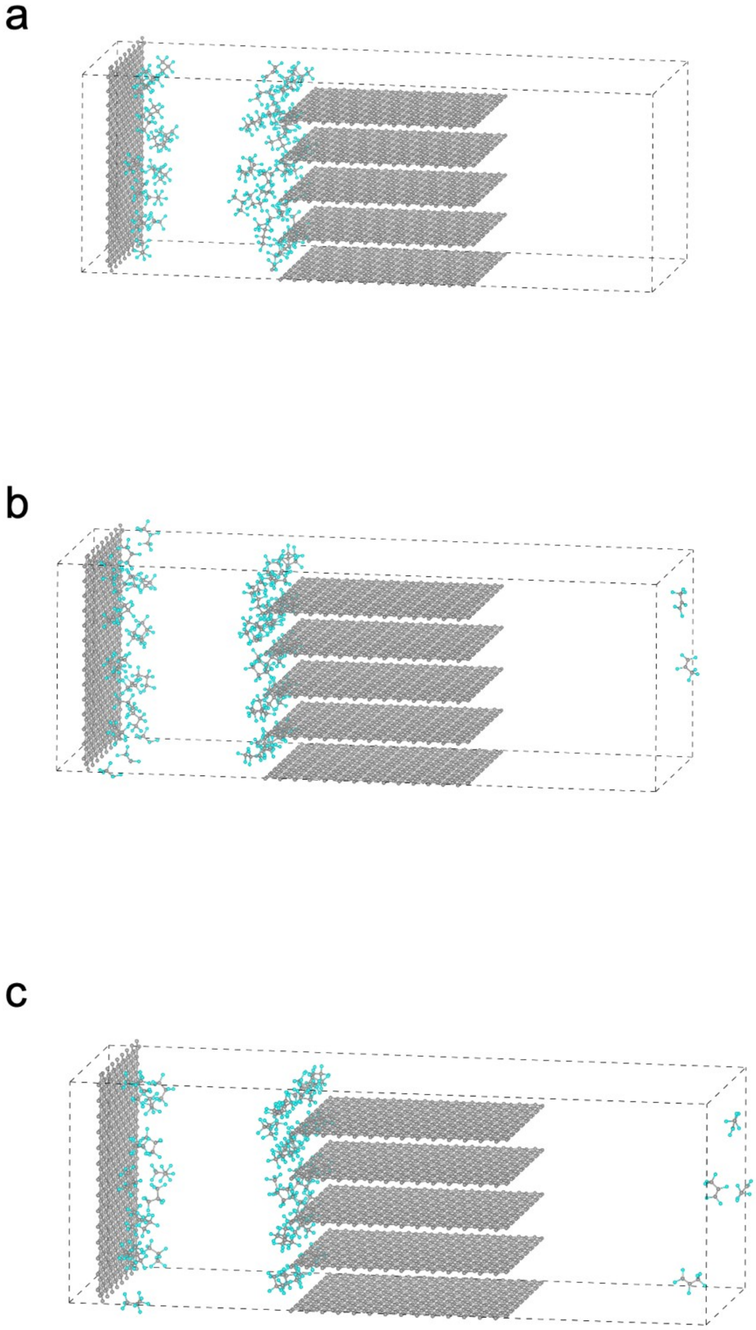

Fig. S13 The number of gas molecules that passed through the PRC-15CO_2 channels in the MD simulation as a function of simulation time: (a) 0 ps; (b) 50 000 ps and (c) 100000 ps.

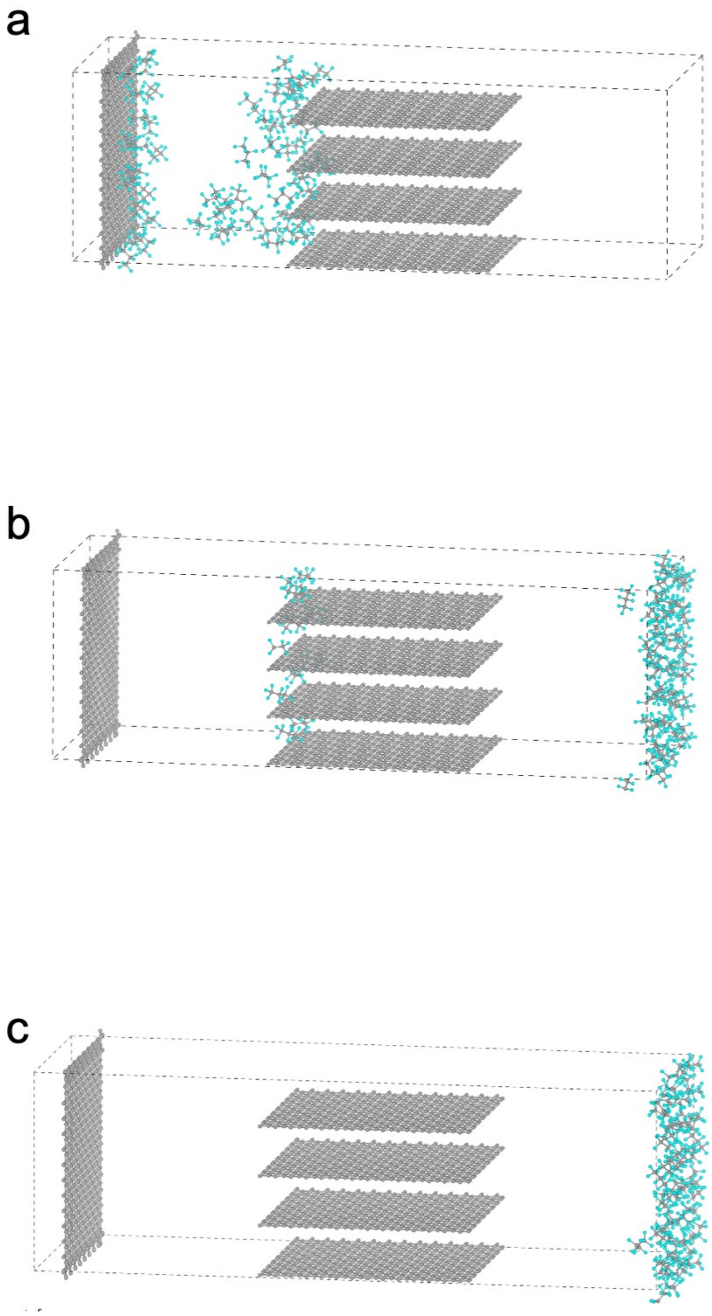

Fig. S14 The number of gas molecules that passed through the PRC-25CO_2 channels in the MD simulation as a function of simulation time: (a) 0 ps; (b) 50 000 ps and (c) 100000 ps.

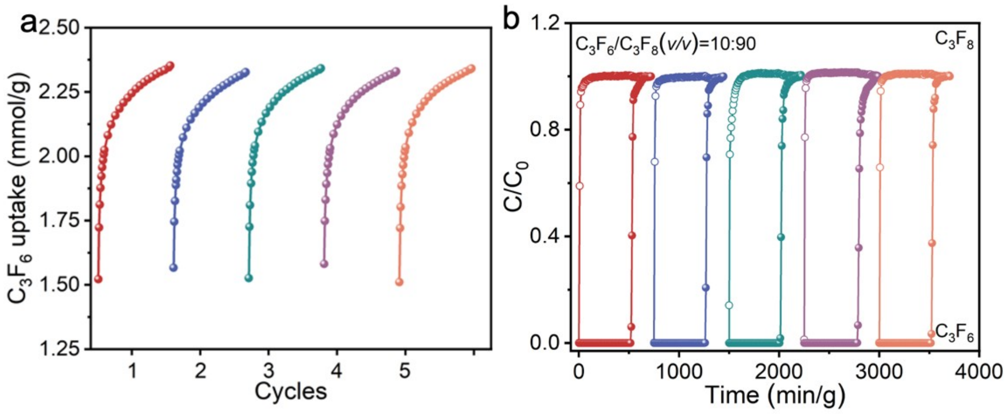

Fig. S15 (a) Five consecutive C_3F_6 adsorption-desorption cycling tests of PRC-15CO_2 at 298 K; (b) Multicycle dynamic breakthrough curves of C_3F_6/C_3F_8 (1/99, *v/v*) gas mixtures using a packed column bed with PRC-15CO_2 at 298 K and 100 kPa.

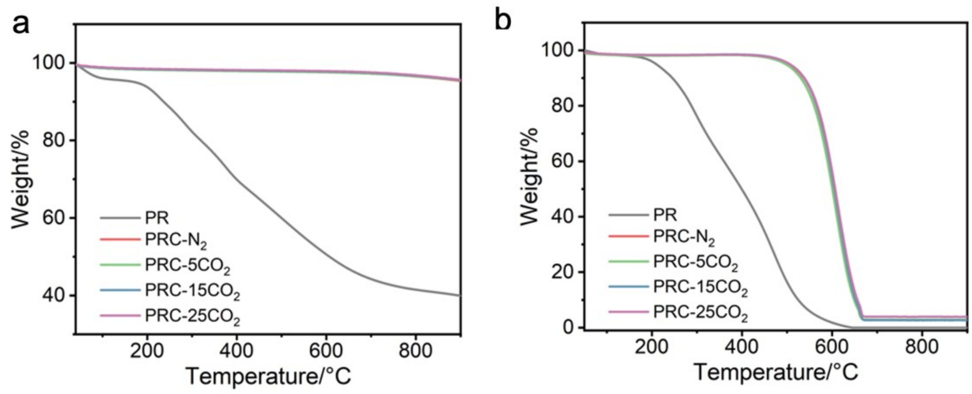

Fig. S16 Thermogravimetric experimental curves of PR and its derived carbon molecular sieve materials under different atmospheres: (a) Nitrogen; (b) Air.

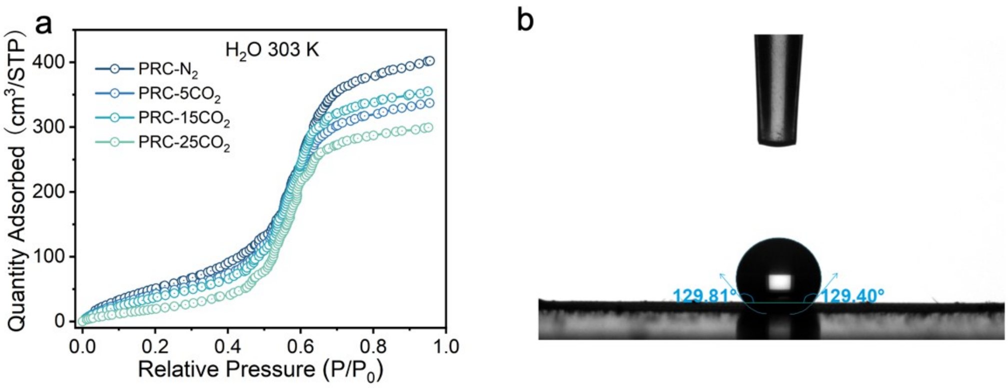

Fig. S17 (a) Adsorption isotherms of water vapor at 303 K on PR derived carbon molecular sieve materials; (b) Water contact angle of PRC-15CO_2.

Fig. S18 Schematic diagram of the amplified synthesis of precursor PR.

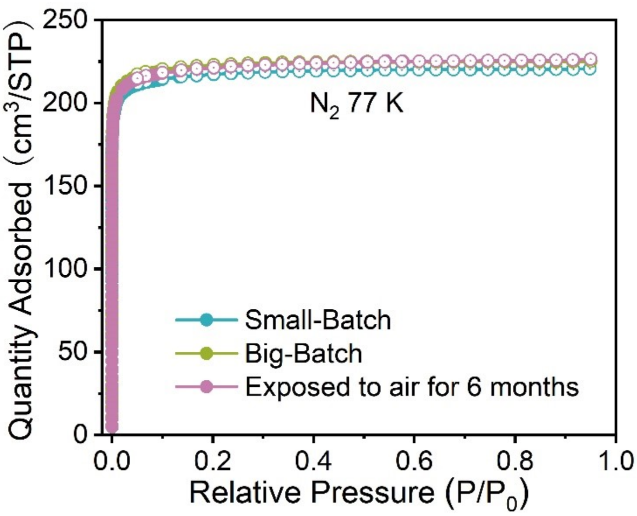

Fig. S19 Comparison of the performance of PRC-15CO_2 synthesized at different conditions: Nitrogen adsorption-desorption curves at 77 K.

Table S1. Elemental analysis results

Sample	C (wt%)	O (wt%)	N (wt%)	H (wt%)	C/O
PR	62.54	22.64	9.43	5.39	2.76
PRC-N_2	94.84	2.28	2.64	0.23	41.54
PRC-5CO_2	95.01	1.01	2.67	1.31	94.37
PRC-15CO_2	95.49	1.64	2.54	0.33	58.13
PRC-25CO_2	94.78	2.33	2.66	0.23	40.66

Table S2. Relative content of peaks in the C_{1s} spectra of the materials

Sample	relative content/%						sp^2C/sp^3C
	sp^2C	sp^3C	C-N	C-O	C=O	O-C=O	
PR	30.22	27.43	21.45	20.90	/	/	1.10
PRC-N_2	60.34	20.41	7.37	4.84	3.16	3.89	2.96
PRC-5CO_2	61.33	19.41	6.21	2.82	3.93	6.32	3.16
PRC-15CO_2	66.49	15.66	4.77	3.39	5.57	4.13	4.25
PRC-25CO_2	70.10	14.87	5.45	3.20	3.31	3.07	4.71

Table S3. Relative content of peaks in the O_{1s} spectra of the materials

Sample	Relative content/%	
	C-O	C=O
PR	60.29	39.71
PRC-N_2	75.41	24.59
PRC-5CO_2	78.98	21.02
PRC-15CO_2	72.71	27.29
PRC-25CO_2	68.37	31.63

Table S4. Relative content of peaks in the N_{1s} spectra of the materials

Sample	Relative content/%			
	External pollution N	Tertiary amine N	Graphitic N	Pyridinic N
PR	15.97	84.03	/	/
PRC-N_2	/	/	84.75	15.25
PRC-5CO_2	/	/	87.5	12.5
PRC-15CO_2	/	/	85.5	14.5
PRC-25CO_2	/	/	86.15	13.85

Table S5. BET specific surface area and pore volume of PR derived carbon materials

	PR-N_2	PR-5CO_2	PR-15CO_2	PR-25CO_2
S_{BET} (m^2 g^{-1})	713.49	793.87	885.80	951.92
V_{total} (cm^3 g^{-1})	0.209	0.250	0.275	0.299
$V_{<7\ Å}$ (cm^3 g^{-1})	0.209	0.231	0.236	0.247

Table S6. Comparison of static adsorption properties of C_3F_6 and C_3F_8 and adsorption capacity ratio of different adsorbent materials at 298 K and 100 kPa

Adsorbent	C_3F_6 uptake (mmol g^{-1})	C_3F_8 uptake (mmol g^{-1})	Uptake ratio	Ref.
PRC-5CO_2	1.162	0.029	40.72	/
PRC-15CO_2	2.336	0.033	70.48	/
PRC-25CO_2	2.765	1.172	2.36	/
AC1	3.496	1.205	2.90	/
AC2	5.246	3.872	1.36	/
AC3	6.896	4.497	1.53	/
AC4	6.006	4.351	1.38	/
AC5	3.906	2.362	1.65	/
AC6	2.663	1.530	1.74	/
CoFA	2.000	0.160	12.5	[1]
Ca-tcpb	2.165	0.0650	33.3	[2]
Zn-bzc-CF_3	2.098	0.089	23.5	[3]
JXNU-21	1.339	0.774	1.73	[4]
Al-PMA	1.750	0.047	37.23	[5]
BASF-300	4.330	3.360	1.29	[6]
BPL-410	4.050	3.032	1.34	[6]
Cu-BTC	5.950	4.500	1.32	[6]
Uio-66	3.167	2.050	1.55	[6]
MIL-53(Al)	3.750	2.670	1.40	[6]
13X	1.970	1.450	1.36	[6]
NaY	2.910	2.000	1.46	[6]
ZSM-5	1.470	0.91	1.62	[6]

Table S7. Diffusion time constants and kinetic selectivity of C_3F_6 and C_3F_8 on materials at 298 K and 100 kPa

Sample	Diffusion time constant (s^{-1})		Kinetic selectivity
	C_3F_6	C_3F_8	
PRC-N_2	/	/	/
PRC-5CO_2	7.49×10^{-5}	molecular sieving	
PRC-15CO_2	9.15×10^{-4}	molecular sieving	
PRC-25CO_2	3.42×10^{-3}	4.02×10^{-4}	8.51

Table S8. Basic information on the separation of C_3F_6/C_3F_8 (10/90, *v/v*) mixtures with different carbon-based adsorbents

Sample	Quality (g)	Breakthrough Time ($min\ g^{-1}$)		Single-pass recovery rate (%)
		C_3F_6	C_3F_8	
PRC-5CO_2	0.4128	92.86	~0	~100.0
PRC-15CO_2	0.4250	218.82	~0	~100.0
PRC-25CO_2	0.4054	222.00	14.80	93.3
AC1	0.5940	136.36	30.30	77.8
AC2	0.4408	142.92	61.25	57.1
AC3	0.4177	136.46	57.46	57.9
AC4	0.4019	149.29	67.18	55.0
AC5	0.4105	102.31	65.77	35.7
AC6	0.6527	45.96	22.98	50.0

Table S9. Summary of separation performance of different carbon-based adsorbents for C_3F_6/C_3F_8 (10/90, *v/v*) mixtures

Sample	Dynamic adsorption uptake ($mmol\ g^{-1}$) C_3F_6	Adsorption loss of C_3F_8 ($L\ kg^{-1}$)	5N C_3F_8 productivity ($L\ kg^{-1}$)
PRC-5CO_2	0.98	~0	167.15
PRC-15CO_2	2.37	~0	393.88
PRC-25CO_2	2.10	26.64	372.96
AC1	1.38	54.54	190.91
AC2	1.78	110.25	147.01

AC3	1.36	103.43	142.20
AC4	1.61	120.92	147.80
AC5	1.44	118.39	65.77
AC6	0.71	41.36	41.36

References

[1] Xia W, Zhou Z, Sheng L, et al. Bioinspired recognition in metal-organic frameworks enabling precise sieving separation of fluorinated propylene and propane mixtures[J]. Nature Communications, 2024, 15(1): 8716.

[2] Xia W, Yang Y, Sheng L, et al. Temperature-dependent molecular sieving of fluorinated propane/propylene mixtures by a flexible-robust metal-organic framework[J]. Science Advances, 2024, 10(3): eadj6473.

[3] Zheng M, Xue W, Yan T, et al. Fluorinated MOF-based hexafluoropropylene nanotrap for highly efficient purification of octafluoropropane electronic specialty gas[J]. Angewandte Chemie International Edition, 2024, 63(15): e202401770.

[4] Feng Y, Ma H, Luo S, et al. Purification of octafluoropropane from hexafluoropropylene/octafluoropropane mixtures with a metal–organic framework exhibiting high productivity[J]. Inorganic Chemistry Frontiers, 2025, 12(2): 623-629.

[5] Xia W, Zhou Z, Sheng L, et al. Deep purification of perfluorinated electronic specialty gas with a scalable metal–organic framework featuring tailored positive potential traps[J]. Science Bulletin, 2025, 70(2): 232-240.

[6] Xia W, Yang Y, Sheng L, et al. Temperature-dependent molecular sieving of fluorinated propane/propylene mixtures by a flexible-robust metal-organic framework[J]. Science Advances, 2024, 10(3): eadj6473.